Journal of Sound and Vibration 632 (2026) 119733

Contents lists available at ScienceDirect

Journal of Sound and Vibration

journal homepage: www.elsevier.com/locate/jsvi

Nonlinear dynamics of rocking rigid blocks under stochastic base excitation: A stochastic-linearization approach

Ioannis P. Mitseas

School of Civil Engineering, University of Leeds, Leeds, LS2 9JT, UK

ARTICLE INFO

Keywords:
Nonlinear dynamics
Random block rocking
Physics-based nonlinear contact law
Stochastic linearization
Uplifting
Lyapunov equation

ABSTRACT

This paper introduces a semi-analytical framework for the nonlinear dynamics of rigid blocks rocking on nonlinear flexible foundations under stochastic base excitation. Unlike classical Housner and Winkler models that assume null or linear base-foundation interaction, the proposed approach incorporates uplift and velocity-dependent dissipation via a Hunt-Crossley-type law, augmented by a tunable cubic restoring component. The foundation is modeled as a distributed bed of nonlinear springs and dampers, combining Winkler-type linear stiffness with added nonlinearity to enable hardening or softening beyond the baseline response. Backbone amplitude dependence arises from contact geometry and is further shaped by the cubic stiffness term. The originally coupled, piecewise nonlinear rocking relations are condensed into a single governing equation using a quasi-static condensation scheme, with smooth analytical surrogates for restoring moment and damping across no-uplift and uplift regimes. A stochastic linearization scheme embedded in Lyapunov moment equations yields time-varying equivalent stiffness and damping, enabling second-order response statistics without repeated integration of highly nonlinear equations. Comparisons with Monte Carlo simulations show close agreement in rotation and rotational velocity variances across excitation intensities and foundation parameters, while achieving significant computational savings. The framework offers an efficient tool for parametric screening of rocking systems under complex soil-structure interaction.

1. Introduction

Rocking of rigid blocks on flexible foundations is intrinsically nonlinear and non-smooth. It emerges in diverse settings from historical monuments, statues and equipment [1,2] to purpose-designed rocking structural components where uplift and partial loss of contact can mitigate force transmission [3–5]. The complexity stems from unilateral contact with the supporting medium, intermittent loss of contact (uplift), and repeated impacts upon reattachment, yielding piecewise governing equations, state-dependent stiffness and damping, and switching between inner (no-uplift) and outer (uplift) regimes. Geometric nonlinearity from the evolving lever arm and compression zone couples with rate-dependent contact dissipation and soil-structure interaction effects (e.g., foundation compliance and yielding). Consequently, the response can exhibit amplitude-dependent backbone hardening or softening, uplift-induced asymmetry, and pronounced state dependence in stiffness and damping. Beyond these deterministic mechanisms, the problem is inherently stochastic [6–8]): ground motions are uncertain and time-varying, contact events occur intermittently, and foundation/interface properties vary in space and time. These features challenge classical linear models such as Housner's model [5,9,10] and the Winkler foundation idealization (e.g., [11–14]), motivating formulations that retain essential contact physics while enabling tractable analysis, uncertainty quantification, and performance-oriented assessment (e.g., [8,15]).

E-mail address: I.Mitseas@leeds.ac.uk

https://doi.org/10.1016/j.jsv.2026.119733
Received 18 November 2025; Received in revised form 10 February 2026; Accepted 24 February 2026
Available online 26 February 2026

Deterministic studies of rigid blocks on rigid foundations dominate the rocking literature, with classical Housner-type formulations and Winkler idealizations setting the baseline for analysis (e.g., [11–14,16])). By comparison, investigations that incorporate foundation flexibility and the associated contact mechanics, uplift, and damping are fewer, though they highlight how compliant bases and interface properties can markedly alter response and even produce counterintuitive trends [17]. Building on this direction, augmented contact laws (e.g., Hunt-Crossley-type model realized as distributed linear springs in parallel with nonlinear dashpots) have been adopted to represent uplift and rate-dependent dissipation in a tractable way (e.g., [18–20]). Researchers favor a representation of the restoring action through a linear law; higher-order polynomial restoring descriptions are, in general, not pursued due to their particulalry cumbersome manipulation under the piecewise contact switching. Within the stochastic setting, the body of work on flexible base-foundation interaction is noticeably smaller (e.g., [19,21–23]).

The present work advances this line of research through an integrated semi-analytical framework for efficient stochastic-response characterization of rocking systems. A generalized distributed contact/soil-structure interaction (SSI) formulation is first introduced, extending the classical Hunt-Crossley-type representation with a compact amplitude-dependent conservative backbone governed by a tunable parameter. This enhancement allows the model to represent both softening (e.g., geometric effects, toe degradation, interface yielding) and hardening trends (e.g., Hertz-type confinement [24]), while recovering the linear-stiffness form adopted in typical Hunt-Crossley rocking formulations as a special case when the parameter vanishes (e.g., [19,22,23,25]). Building on this formulation, a tailored stochastic linearization procedure [26–28] is developed to obtain closed-form, time-varying equivalent stiffness and damping and to embed them within a unified Lyapunov-based covariance propagation scheme for stochastic base inputs, covering both modulated unfiltered white noise and its filtered counterpart within a compact state-space description [27]. The resulting equivalent coefficients are time-dependent and physically interpretable, as they encode the evolving mixture of no-uplift and uplift states alongside the concurrent influence of rate-dependent dissipation and amplitude-dependent conservative restoring shifts.

The proposed methodology delivers time-varying variances of rotation and rotational velocity without repeated nonlinear time integration of the governing rocking equations, enabling orders-of-magnitude computational savings relative to Monte Carlo simulation (MCS) when ensemble statistics are sought, while maintaining adequate agreement for the range of excitation levels and foundation parameters examined. Moreover, by explicitly nesting prevalent models as limiting cases-Winkler as the fully linear case, Hunt-Crossley with linear restoring as a commonly used intermediate, and the present generalized law as the encompassing case-the formulation remains parsimonious and offers a transparent basis for model selection and subsequent parameter identification/calibration against laboratory tests or field records.

In the remainder of this paper, Sections 2.1 through 2.6 develop the mathematical foundations underpinning the proposed semi-analytical stochastic rocking dynamics framework. Section 2.7 discusses salient attributes of the method, including its strengths and limitations. Sections 3.1 to 3.2 present representative case studies across multiple excitation intensities and stiffness-nonlinearity configurations (hardening/softening) for rigid blocks on nonlinear flexible foundations subjected to time modulated unfiltered and filtered white-noise excitations. The accuracy and reliability of the approach are assessed by comparison with MCS results from nonlinear response-history analysis (NRHA). Section 3.3 offers remarks on the results, and Section 4 synthesizes the main findings and outlines broader implications.

2. Mathematical formulation

This section elaborates the mathematical edifice of the proposed semi-analytical stochastic dynamics framework for efficiently evaluating second-order response statistics without recourse to repeated integration of the coupled, piecewise, nonlinear equations of rocking. It formalizes the governing hypotheses, codifies the base-foundation idealizations, including uplift and a sophisticated physics-based nonlinear stiffness-damping law, and delineates the solution sequence involving static condensation followed by stochastic linearization within a Lyapunov setting that preserves the essential physics across no-uplift and uplift regimes while rendering the problem analytically tractable.

2.1. Base-foundation: physics-based nonlinear stiffness-damping law

Traditional rigid-block rocking models span from Housner-type rigid-contact formulations [9,10] to compliant Winkler-foundation representations [11–14,16], and are often augmented with Hunt-Crossley-type dissipation while retaining a linear restoring component [19,21–23,25]. Although these models provide a practical and analytically tractable basis in many applications, the linear-backbone assumption may be restrictive when unilateral contact effects become pronounced. In particular, migration and shortening of the compression zone, evolution of the effective lever arm with rotation, and phenomena such as toe degradation or interface yielding can introduce amplitude-dependent restoring characteristics that are not reproducible through nonlinear damping calibration alone. This motivates contact/SSI descriptions that retain analytical manageability while allowing an explicitly amplitude-dependent conservative backbone.

The present study therefore introduces a generalized physics-based contact law on a continuously distributed spring-damper bed that combines linear and nonlinear stiffness components with Hunt-Crossley-type rate-dependent dissipation. Crucially, the formulation nests prevalent models as limits: Winkler emerges as the fully linear case; Hunt-Crossley with linear restoring appears as a common intermediate; and the proposed generalized contact law encompasses both, while enabling amplitude-dependent hardening/softening and uplift-induced asymmetry that elude purely linear restoring assumptions. A notable feature of the proposed law, consistent with the interpretation of Gilardi and Sharf [20], is that the damping term depends not only on the local deformation

rate but also on the local deformation, thereby accounting for the progressive increase of the contact area with compression. This dependence ensures that the normal contact force evolves smoothly during impact and separation, starting from zero at initial contact and returning to zero upon detachment, eliminating artificial discontinuities typical of simpler models.

Building on the proposed formulation, the foundation is idealized here as a continuously distributed and independent parallel nonlinear springs and dampers bed along the block base (Fig. 1). Let $\eta \in [0, 2b]$ denote the abscissa measured from the rocking edge B, and let $z(\eta, t) > 0$ be the local indentation with local vertical rate $\dot{z}(\eta, t)$. For a rigid block,

$$z(\eta, t) = z_B(t) - \eta \sin\theta(t), \qquad \dot{z}(\eta, t) = \dot{z}_B(t) - \eta\,\dot{\theta}(t)\cos\theta(t) \tag{1}$$

with

$$z_B(t) = z_{\rm cb} + b\sin\theta(t) \tag{2}$$

being the vertical displacement of the base edge B and $\theta(t)$ the rocking rotation (positive clockwise - Fig. 1(a) and (b)); the subscript cb stands for the center of base. To capture nonlinear amplitude effects beyond linear stiffness while retaining the proven rate-dependent dissipation of Hunt-Crossley kind, the normal contact force per unit length is postulated as

$$F_n(\eta, t, \varepsilon) \;=\; k\, z(\eta, t) + \varepsilon\, k\, z(\eta, t)^3 + \lambda\, z(\eta, t)\dot{z}(\eta, t) \tag{3}$$

with

$$F_n(\eta, t, \varepsilon) = 0 \text{ when } z(\eta, t) < 0 \tag{4}$$

where $k > 0$ and $\lambda > 0$ are the stiffness and damping coefficients per unit width, and $\varepsilon \in \mathbb{R}$ is a tuning parameter that governs the magnitude and sign of the cubic restoring nonlinearity. Setting $\varepsilon = 0$ recovers the common intermediate Hunt-Crossley model used in a number of current studies [19,21–23], while $\varepsilon > 0$ ($\varepsilon < 0$) induces hardening (softening) of the backbone, consistent with Hertz-type nonlinear elasticity and damage-/geometry-induced stiffness variation. Note that the case of the traditional Winkler Foundation Model (WFM), characterized by the linear relation $F_n(\eta, t) = k\, z(\eta, t) + c\, \dot{z}(\eta, t)$ could be seen as a special case of the proposed model. Let $[\eta_I(t), \eta_U(t)] \subseteq [0, 2b]$ be the instantaneous contact interval determined by the unilateral constraint. The resultant vertical force and the moment about the base center are expressed in the general case as

$$F_{\rm cb}(t) = \int_{\eta_I(t)}^{\eta_U(t)} F_n(\eta, t, \varepsilon)\, {\rm d}\eta \tag{5}$$

and

$$M_{\rm cb}(t) = \int_{\eta_I(t)}^{\eta_U(t)} F_n(\eta, t, \varepsilon)\left[(b - \eta)\cos\theta(t)\right] {\rm d}\eta \tag{6}$$

where for the no-uplift regime the limits are $\eta_I = 0$, $\eta_U = 2b$; in uplift they contract according to the instantaneous compression zone, as in the classical distributed-contact formulation; for positive clockwise rotation shown in Fig. 1(c) the limits are $\eta_U = z_{\rm cb}/\sin\theta + b$. Two distinct contact regimes are admissible. Uplift begins the moment either pivot (A or B) detaches from the ground. No-uplift prevails as long as the entire base remains into the ground (see Fig. 1(a) and (b)). This dichotomy is a key departure from rigid-foundation idealizations, for which detachment cannot be represented and the base is assumed to remain fully supported at all times.

2.2. Rocking kinematics and equations of motion

This subsection revisits the dynamics of a rectangular rigid block rocking on a nonlinear flexible foundation under evolutionary stochastic base excitation, following the general lines of Spanos et al. [19], Mitseas et al. [23]. Let m be the block mass, h half of its height, and $I_{\rm cm}$ the polar moment of inertia around the center of mass. Denote by $z_{\rm cb}(t)$ the vertical displacement of the base center and by $\theta(t)$ the rotation, with positive θ corresponding to uplift at the left toe. The ground motion is modeled through horizontal and vertical base accelerations $\ddot{x}_g(t)$ and $\ddot{z}_g(t)$, respectively. The coupled rotational equations governing the dynamic balances read

$$m\,\ddot{z}_{cb} + mh\big(\dot{\theta}^2\cos\theta + \ddot{\theta}\sin\theta\big) + F_{\rm cb} - mg = m\,\ddot{z}_g \tag{7}$$

$$\big(I_{\rm cm} + mh^2\big)\,\ddot{\theta} + M_{\rm cb} + mh\big(\ddot{z}_{cb} - g\big)\sin\theta = mh\big(\ddot{x}_g\cos\theta - \ddot{z}_g\sin\theta\big) \tag{8}$$

where g is gravity acceleration; $F_{\rm cb}$ and $M_{\rm cb}$ denote, respectively, the resultant vertical contact force and the contact moment with respect to the base center. The latter quantities depend on the unilateral block-foundation interaction described via the generalized Hunt-Crossley law, augmented by a tunable cubic nonlinear restoring component, proposed in Subection 2.1. When both base corners remain in contact with the ground level, $F_{\rm cb}$ and $M_{\rm cb}$ can be described for the no-uplifting regime as

$$F_{\rm cb}^{\text{no-uplift}} \;=\; 2bk\, z_{\rm cb} + 2b\,\varepsilon\, k\, z_{\rm cb}\big(z_{\rm cb}^2 + b^2\sin^2\theta\big) + b\lambda\Big(\tfrac{1}{3}b^2\dot{\theta}\sin 2\theta + 2z_{\rm cb}\dot{z}_{cb}\Big) \tag{9}$$

and

$$M_{\rm cb}^{\text{no-uplift}} \;=\; \tfrac{2}{3}b^3 k\sin\theta\cos\theta + \varepsilon k\cos\theta\Big(2z_{\rm cb}^2\sin\theta\, b^3 + \tfrac{2}{5}\sin^3\theta\, b^5\Big) + \tfrac{2}{3}\lambda b^3\big(z_{\rm cb}\dot{\theta}\cos^2\theta + \dot{z}_{cb}\sin\theta\cos\theta\big) \tag{10}$$

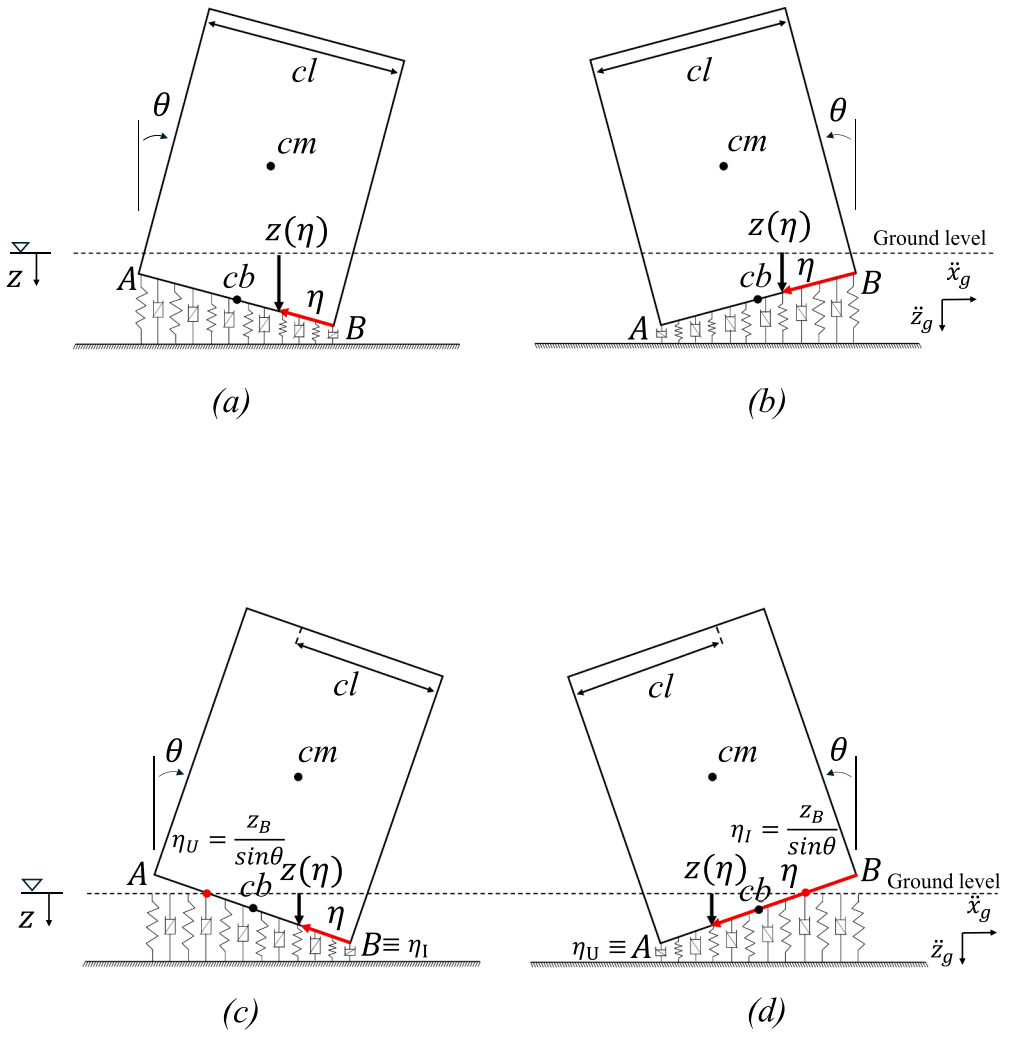

Fig. 1. Block rocking on nonlinear flexible foundation: (a) no-uplifting with $\theta > 0$; (b) no-uplifting with $\theta < 0$; and (c) uplifting with $\theta > 0$; (d) uplifting with $\theta < 0$. Definition of the contact line (cl) for each case.

Once one pivot lifts off the ground, the compression region localizes near the engaged base corner. In that uplifting regime,

$$F_{\mathrm{cb}}^{\mathrm{uplift}} = \frac{k}{2\,|\sin\theta|}\left(b\sin\theta + z_{\mathrm{cb}}\right)^2 + \frac{\varepsilon\,k}{4\,|\sin\theta|}\left(b\sin\theta + z_{\mathrm{cb}}\right)^4 + \frac{\lambda}{6\,|\sin\theta|^2}\left(b\sin\theta + z_{\mathrm{cb}}\right)^2\left[b\,\dot{\theta}\,\sin 2\theta - \dot{z}_{cb}\,\cos\theta + 3\,\dot{z}_{cb}\,\sin\theta\right] \tag{11}$$

and

$$M_{\mathrm{cb}}^{\mathrm{uplift}} = \frac{k\left(b\sin\theta + z_{\mathrm{cb}}\right)^2\left(2b\sin\theta - z_{\mathrm{cb}}\right)\cos\theta}{6\,|\sin\theta|^2} + \frac{\varepsilon\,k\left(b\sin\theta + z_{\mathrm{cb}}\right)^4\left(4b\sin\theta - z_{\mathrm{cb}}\right)\cos\theta}{20\,|\sin\theta|^2} + \frac{\lambda\cos\theta}{12\,|\sin\theta|^3}\left[\dot{\theta}\left(3b^4\sin^4\theta + 4b^3 z_{\mathrm{cb}}\sin^3\theta + z_{\mathrm{cb}}^4\right) + 2\dot{z}_{cb}\left(b\sin\theta + z_{\mathrm{cb}}\right)^2\left(2b\sin\theta - z_{\mathrm{cb}}\right)\sin\theta\right] \tag{12}$$

In Eqs. (9)–(12), b is the half-width of the base; k (force per unit base width per unit indentation) and λ (force per unit base width per unit indentation-velocity and per unit indentation) are, respectively, the stiffness and damping coefficients of the distributed contact; and ε is a single tunable parameter governing the behavior of the nonlinear stiffness contribution. The two regimes namely no-uplift and uplift, are selected kinematically: the former applies while the full base remains in contact; the latter is activated as soon as either pivot rises above the ground.

2.3. Efficient rocking equations decoupling via a quasi-static condensation method

In most practical cases, both the rotational angle θ and the vertical displacement z_{cb} remain within small to moderate bounds (e.g., [12,19,23]), allowing the adoption of the small-angle approximations $\sin\theta \approx \theta$ and $\cos\theta \approx 1$. Further simplifications can be introduced

by neglecting higher-order coupling terms involving derivatives of θ and $z_{\rm cb}$ whose combined order exceeds one, as their influence on the system dynamics is typically negligible. The external excitation is assumed to act purely in the horizontal direction, with $\ddot{z}_g = 0$ and a nonzero horizontal acceleration component $\ddot{x}_g$. Under these assumptions, and considering Eqs. (7) to (12), the formulation yields a redefined set of nonlinear rocking equations that provide a more tractable yet physically consistent representation of the system's motion for the no-uplift

$$m\ddot{z}_{cb} + 2b\lambda z_{\rm cb}\dot{z}_{cb} + 2bkz_{\rm cb} + 2b\epsilon k z_{\rm cb}(z_{\rm cb}^2 + b^2\theta^2) + \frac{2}{3}b^3\lambda\theta\dot{\theta} = mg \tag{13}$$

and

$$(I_{\rm cm}+mh^2)\ddot{\theta} + \frac{2}{3}b^3k\theta + \epsilon k\left(2z_{\rm cb}^2 b^3\theta + \frac{2}{5}b^5\theta^3\right) + \frac{2}{3}\lambda b^3\left(z_{\rm cb}\dot{\theta} + \dot{z}_{cb}\theta\right) - mhg\theta = mh\ddot{x}_g \tag{14}$$

and uplift regimes, respectively.

$$m\ddot{z}_{cb} + \frac{k}{2|\theta|}(b\theta + z_{\rm cb})^2 + \frac{\epsilon k}{4|\theta|}(b\theta + z_{\rm cb})^4 + \frac{\lambda}{6\theta^2}(b\theta + z_{\rm cb})^2\left(2b\theta\dot{\theta} - \dot{z}_{cb} + 3\dot{z}_{cb}\theta\right) = mg \tag{15}$$

and

$$\begin{aligned}(I_{\rm cm} + mh^2)\,\ddot{\theta} + &\frac{k\,(b\theta + z_{\rm cb})^2\,(2b\theta - z_{\rm cb})}{6\,\theta^2} + \frac{\epsilon\,k\,(b\theta + z_{\rm cb})^4\,(4b\theta - z_{\rm cb})}{20\,\theta^2} + \frac{\lambda}{12\,|\theta|^3}\Big[\dot{\theta}\left(3b^4\theta^4 + 4b^3 z_{\rm cb}\,\theta^3 + z_{\rm cb}^4\right)\\ &+2\,\dot{z}_{cb}\,(b\theta + z_{\rm cb})^2\,(2b\theta - z_{\rm cb})\,\theta\Big] - mhg\,\theta = mh\,\ddot{x}_g\end{aligned} \tag{16}$$

Employing an approximative static condensation approach [6,23] subsequently reduces the originally coupled governing relations, Eqs. (7) and (8), to a single rocking equation characterized by piecewise, state-dependent nonlinear stiffness and nonlinear damping properties. The proposed simplification is appropriate for the scope of the present study, which concentrates on systems exhibiting soft to moderate levels of stiffness nonlinearity. This reduced formulation preserves the essential nonlinear coupling between uplift and rocking while offering a compact yet accurate representation suitable for analytical derivations and efficient numerical implementation. In this regard, considering the quasi-static condensation method yields

$$z_{\rm cb}^{\text{no-uplift}} = z_{\rm st} \approx \frac{mg}{2bk} \tag{17}$$

for the case of no-uplifting, and

$$z_{\rm cb}^{\text{uplift}} = z_{\rm st} \approx \sqrt{\frac{2mg|\theta|}{k}} - b|\theta| \tag{18}$$

for the case of uplifting. Note that under static conditions, uplifting occurs when $|\theta| > \theta_{\rm ul}$, where $\theta_{\rm ul}$ denotes the uplift initiation threshold angle

$$\theta_{\rm ul} = \frac{|z_{\rm st}|}{b} = \frac{mg}{2b^2k} \tag{19}$$

Upon substituting Eqs. (17) and (18) into Eqs. (14) and (16), the governing relations take the following form

$$(I_{\rm cm} + mh^2)\ddot{\theta} + \left(\frac{\lambda b^2 mg}{3k}\right)\dot{\theta} + \left\{\frac{2}{3}b^3k + \varepsilon\left(\frac{m^2g^2b}{2k} + \frac{2}{5}kb^5\theta^2\right) - mhg\right\}\theta = mh\ddot{x}_g \tag{20}$$

and

$$\left(I_{\rm cm} + mh^2\right)\ddot{\theta} + \frac{\lambda b}{12}\left(\frac{2mg}{k}\right)^{\frac{3}{2}}|\theta|^{-\frac{1}{2}}\dot{\theta} + \left[\frac{mg\,b}{|\theta|} - \frac{mg}{3}\sqrt{\frac{2mg}{k}}\,|\theta|^{-\frac{3}{2}} - \frac{\varepsilon m^2g^2}{5k}\sqrt{\frac{2mg}{k}}\,|\theta|^{-\frac{1}{2}} + \left(\frac{\varepsilon m^2g^2b}{k} - mgh\right)\right]\theta = mh\ddot{x}_g \tag{21}$$

Subsequently, Eq. (20) and (21) can be recast in the form

$$m_{\rm sdof}\ddot{\theta} + C(\theta)\dot{\theta} + K(\theta)\theta = mh\ddot{x}_g \tag{22}$$

where

$$m_{\rm sdof} = I_{\rm cm} + mh^2 \tag{23}$$

$$C(\theta) = \begin{cases} \dfrac{\lambda b^2 mg}{3k}, & |\theta| \le \theta_{\rm ul} \\ \dfrac{\lambda b}{12}\left(\dfrac{2mg}{k}\right)^{\frac{3}{2}}|\theta|^{-\frac{1}{2}}, & |\theta| > \theta_{\rm ul} \end{cases} \tag{24}$$

and

$$K(\theta)=\begin{cases}\dfrac{2}{3}\,b^3k\;-\;mgh+\;\varepsilon\left(\dfrac{m^2g^2b}{2k}+\dfrac{2}{5}\,k\,b^5\,\theta^2\right), & |\theta|\le\theta_{\mathrm{ul}}\\ mg\left(\dfrac{b}{|\theta|}-\dfrac{1}{3k}\sqrt{2mgk}\;|\theta|^{-3/2}-h\right)+\;\varepsilon\left(\dfrac{m^2g^2b}{k}-\dfrac{m^2g^2}{5k}\sqrt{\dfrac{2mg}{k}}\;|\theta|^{-1/2}\right), & |\theta|>\theta_{\mathrm{ul}}\end{cases} \tag{25}$$

Notably, the dynamics in Eqs. (22)–(25) are governed by twofold nonlinearity: both the stiffness and damping components evolve and switch as the response transitions between the no-uplift and uplift regimes.

2.4. System stochastic linearization framework

The nonlinear single-degree-of-freedom (SDOF) system defined in Eq. (22) exhibits piecewise, state-dependent nonlinear behavior through the functions $C(\theta)$ and $K(\theta)$ provided in Eqs. (24) and (25). To investigate the stochastic response of this system under random base excitation, the equivalent stochastic linearization method is employed. In the ensuing analysis, the rotational response $\theta(t)$ is considered to be a stationary, zero-mean Gaussian process. This assumption is commonly adopted in the study of lightly nonlinear systems subjected to broadband random excitation, as it allows for analytical tractability while retaining physical relevance. Based on this assumption, an equivalent linearized model is formulated as

$$m_{\mathrm{sdof}}\ddot{\theta}+c_{\mathrm{eq}}(t)\dot{\theta}+k_{\mathrm{eq}}(t)\theta=mh\ddot{x}_g \tag{26}$$

where $c_{\mathrm{eq}}(t)$ and $k_{\mathrm{eq}}(t)$ denote the equivalent time-dependent damping and stiffness coefficients, respectively. These coefficients are determined by minimizing the mean-square error between the nonlinear and equivalent linearized system of Eqs. (22) and (26). Following the piecewise formulation of $C(\theta)$ and $K(\theta)$ in Eqs. (24) and (25), smooth approximations are introduced using a transition function $f(\theta)$, such that

$$C_{\mathrm{aux}}(\theta)=f(\theta)C_1(\theta)+[1-f(\theta)]C_2(\theta) \tag{27}$$

and

$$K_{\mathrm{aux}}(\theta)=f(\theta)K_1(\theta)+[1-f(\theta)]K_2(\theta) \tag{28}$$

where $C_1(\theta)$ and $K_1(\theta)$ correspond to the no-uplift regime (inner), and $C_2(\theta)$ and $K_2(\theta)$ correspond to the uplift regime (outer) of the original nonlinear system. The transition function $f(\theta)$ is defined by

$$f(\theta)=H(\theta+\theta_{\mathrm{ul}})-H(\theta-\theta_{\mathrm{ul}}) \tag{29}$$

where H is the Heaviside step function. Based on the original definition of Eq. (22), the auxiliary compact form of the equation of motion is expressed as

$$m_{\mathrm{sdof}}\ddot{\theta}+C_{\mathrm{aux}}(\theta)\dot{\theta}+K_{\mathrm{aux}}(\theta)\theta=mh\ddot{x}_g \tag{30}$$

The equivalent linearized coefficients of Eq. (26) with respect to the compact formulation of Eq. (30) are defined as (e.g., [27,29])

$$c_{\mathrm{eq}}(t)=\mathbb{E}\left[\frac{\partial g(\theta,\dot{\theta})}{\partial\dot{\theta}}\right],\qquad k_{\mathrm{eq}}(t)=\mathbb{E}\left[\frac{\partial g(\theta,\dot{\theta})}{\partial\theta}\right] \tag{31}$$

where

$$g(\theta,\dot{\theta})=C_{\mathrm{aux}}(\theta)\,\dot{\theta}+K_{\mathrm{aux}}(\theta)\,\theta=\left\{f(\theta)C_1(\theta)+[1-f(\theta)]C_2(\theta)\right\}\dot{\theta}+\left\{f(\theta)K_1(\theta)+[1-f(\theta)]K_2(\theta)\right\}\theta \tag{32}$$

Assuming that $\theta(t)$ and $\dot{\theta}(t)$ can be approximated as Gaussian processes, the marginal probability density function (PDF) of $\theta(t)$ is expressed as

$$p_\theta(\theta)=\frac{1}{\sqrt{2\pi}\sigma_\theta}\exp\left(-\frac{\theta^2}{2\sigma_\theta^2}\right) \tag{33}$$

and the corresponding joint PDF of $\theta(t)$ and $\dot{\theta}(t)$ is given by

$$p_{\theta\dot{\theta}}=\frac{1}{2\pi\sigma_\theta\sigma_{\dot{\theta}}\sqrt{1-\rho^2}}\exp\left[-\frac{1}{(1-\rho^2)}\frac{\sigma_{\dot{\theta}}^2\theta^2-2\rho\sigma_\theta\sigma_{\dot{\theta}}\theta\dot{\theta}+\sigma_\theta^2\dot{\theta}^2}{2\sigma_\theta^2\sigma_{\dot{\theta}}^2}\right] \tag{34}$$

where σ_θ and $\sigma_{\dot{\theta}}$ denote the standard deviations of $\theta(t)$ and $\dot{\theta}(t)$, respectively, and ρ is their correlation coefficient. Under these assumptions, the expectations in Eq. (31) can be evaluated analytically, yielding closed-form analytical expressions for the equivalent time-dependent damping and stiffness coefficients:

$$c_{\mathrm{eq}}(t)=\frac{\lambda\,b^2\,m\,g}{3k}\;\mathrm{erf}\!\left(\frac{\theta_{\mathrm{ul}}}{\sqrt{2}\,\sigma_\theta}\right)\;+\;\frac{\lambda\,b}{12}\left(\frac{2mg}{k}\right)^{\frac{3}{2}}\frac{2^{-1/4}}{\sqrt{\pi}\,\sigma_\theta^{1/2}}\,\Gamma\!\left(\frac{1}{4},\,\frac{\theta_{\mathrm{ul}}^2}{2\,\sigma_\theta^2}\right) \tag{35}$$

and

$$k_{\mathrm{eq}}(t) = -mgh + \frac{b}{3\,\sigma_\theta}\sqrt{\frac{2}{\pi}}\,\exp\!\Big(-\frac{\theta_{\mathrm{ul}}^2}{2\,\sigma_\theta^2}\Big)\Big(3mg - 2b^2 k\,\theta_{\mathrm{ul}}\Big) + \frac{2}{3}\,b^3 k\,\mathrm{erf}\Big(\frac{\theta_{\mathrm{ul}}}{\sqrt{2}\,\sigma_\theta}\Big) - \frac{1}{3}\,\frac{mg}{k\sqrt{\pi}}\,\frac{2^{3/4}\sqrt{mgk}}{\sigma_\theta^{3/2}}\,\Gamma\Big(\frac{3}{4},\,\frac{\theta_{\mathrm{ul}}^2}{2\,\sigma_\theta^2}\Big)$$
$$-\frac{b\,mg}{12\,k^2\sqrt{\pi}}\,\lambda\,\rho\,\frac{\sigma_{\dot\theta}}{\sigma_\theta^{3/2}}\,2^{1/4}\sqrt{mgk}\,\Gamma\Big(\frac{1}{4},\,\frac{\theta_{\mathrm{ul}}^2}{2\,\sigma_\theta^2}\Big) + \frac{b\,mg}{3\,k^2\sqrt{\pi}}\,\lambda\,\rho\,\frac{\sigma_{\dot\theta}}{\sigma_{\dot\theta}^2}\,\exp\!\Big(-\frac{\theta_{\mathrm{ul}}^2}{2\,\sigma_\theta^2}\Big)\Big(\sqrt{mgk\,\theta_{\mathrm{ul}}} - \sqrt{2}\,bk\,\theta_{\mathrm{ul}}\Big)$$
$$+\varepsilon\Bigg[\frac{m^2g^2b}{2k}\,\mathrm{erf}\Big(\frac{\theta_{\mathrm{ul}}}{\sqrt{2}\,\sigma_\theta}\Big) + \frac{2}{5}\,k\,b^5\Big(\sigma_\theta^2\,\mathrm{erf}\Big(\frac{\theta_{\mathrm{ul}}}{\sqrt{2}\,\sigma_\theta}\Big) - \sqrt{\frac{2}{\pi}}\,\sigma_\theta\,\theta_{\mathrm{ul}}\,\exp\!\Big(-\frac{\theta_{\mathrm{ul}}^2}{2\,\sigma_\theta^2}\Big)\Big)\Big)$$
$$+\frac{m^2g^2b}{k}\,\mathrm{erfc}\Big(\frac{\theta_{\mathrm{ul}}}{\sqrt{2}\,\sigma_\theta}\Big) - \frac{m^2g^2}{5k}\sqrt{\frac{2mg}{k}}\,\frac{2^{-1/4}}{\sqrt{\pi}\,\sigma_\theta^{1/2}}\,\Gamma\Big(\frac{1}{4},\,\frac{\theta_{\mathrm{ul}}^2}{2\,\sigma_\theta^2}\Big)\Bigg] \tag{36}$$

The error function and its complement are defined by

$$\mathrm{erf}(x) = \frac{2}{\sqrt{\pi}}\int_0^x e^{-t^2}\,\mathrm{d}t, \qquad \mathrm{erfc}(x) = 1 - \mathrm{erf}(x) = \frac{2}{\sqrt{\pi}}\int_x^\infty e^{-t^2}\,\mathrm{d}t \tag{37}$$

whereas the upper incomplete Gamma function [30] is

$$\Gamma(a,x) = \int_x^\infty t^{a-1}e^{-t}\,\mathrm{d}t, \qquad a>0,\ x\geq 0 \tag{38}$$

which generalizes the ordinary Gamma function $\Gamma(a) = \Gamma(a,0)$. In this work $\Gamma(\cdot,\cdot)$ appears with fractional orders (e.g., $a = \frac{1}{4}, \frac{3}{4}$) from tail integrals of power- exponential kernels arising in the uplift regime. These functions are standard, smooth, and numerically well-conditioned for the parameter ranges considered.

2.5. Lyapunov formulation for time-modulated unfiltered white noise excitation

The horizontal base acceleration is modeled as a zero-mean, Gaussian white noise $\xi(t)$ with one-sided spectral density $2\pi S_0$, modulated by a deterministic envelope time function $q(t)$

$$\ddot{x}_g(t) = q(t)\,\xi(t), \qquad \mathbb{E}\big[\xi(t)\xi(\tau)\big] = 2\pi S_0\,\delta(t-\tau) \tag{39}$$

where $\delta(\cdot)$ is the Dirac delta function. The governing rocking dynamics can be defined in a time-varying state-space form [27,31] as

$$\dot{\mathbf{y}}(t) = \mathbf{P}(t)\,\mathbf{y}(t) + \mathbf{v}(t) \tag{40}$$

with state vector, system matrix, and input vector

$$\mathbf{y}(t) = \big[\,\theta(t)\ \ \dot\theta(t)\,\big]^{\mathsf{T}} \tag{41}$$

$$\mathbf{P}(t) = \begin{bmatrix} 0 & 1 \\ -\dfrac{k_{\mathrm{eq}}(t)}{m_{\mathrm{sdof}}} & -\dfrac{c_{\mathrm{eq}}(t)}{m_{\mathrm{sdof}}} \end{bmatrix} \tag{42}$$

and

$$\mathbf{v}(t) = \Big[\,0\ \ \frac{mh\,q(t)\,\xi(t)}{m_{\mathrm{sdof}}}\,\Big]^{\mathsf{T}} \tag{43}$$

Let $\mathbf{C}(t) = \mathbb{E}\big[\mathbf{y}(t)\mathbf{y}^T(t)\big]$ denote the covariance matrix,

$$\mathbf{C}(t) = \begin{bmatrix} \sigma_\theta^2 & \sigma_{\theta\dot\theta} \\ \sigma_{\theta\dot\theta} & \sigma_{\dot\theta}^2 \end{bmatrix} \tag{44}$$

For Gaussian, delta-correlated excitation, $\mathbf{C}(t)$ evolves according to the Lyapunov moment equation

$$\dot{\mathbf{C}} = \mathbf{P}\,\mathbf{C} + \mathbf{C}\,\mathbf{P}^T + \mathbb{E}\big[\mathbf{v}\,\mathbf{v}^T\big] \tag{45}$$

with driving term

$$\mathbb{E}\big[\mathbf{v}(t)\,\mathbf{v}^T(t)\big] = \begin{bmatrix} 0 & 0 \\ 0 & 2\pi S_0\Big(\dfrac{m\,h\,q(t)}{m_{\mathrm{sdof}}}\Big)^2 \end{bmatrix} \tag{46}$$

At each time instant t, the pair $(\sigma_\theta^2, \sigma_{\dot\theta}^2)$ and correlation $\rho = \sigma_{\theta\dot\theta}/(\sigma_\theta\sigma_{\dot\theta})$ define the Gaussian surrogate of Eq. (30). Using these moments, the expressions of Eqs. (35) and (36) yield updated $c_{\mathrm{eq}}(t)$ and $k_{\mathrm{eq}}(t)$ in closed form. The Lyapunov ordinary differential equation

(ODE) Eq. (45) is then numerically integrated forward over the current time step. This fixed-point update (moments → equivalent coefficients → moments) is iterated at each time step until convergence, furnishing the time-varying second-order response statistics without direct integration of the original nonlinear equations of motion, Eqs. (7) to (12).

2.6. Lyapunov formulation for time-modulated filtered white noise excitation

The ground acceleration in the modulated form reads

$$\ddot{x}_g(t) = q(t)\, z(t) \tag{47}$$

where $z(t)$ is the output of a second-order linear filter of the Kanai-Tajimi type (e.g., [32,33]), driven by white noise $\xi(t)$

$$z(t) = -2\zeta_g\omega_g\, \dot{u}_g(t) \; - \; \omega_g^2\, u_g(t) \tag{48}$$

where

$$\ddot{u}_g(t) \; + \; 2\zeta_g\omega_g\, \dot{u}_g(t) \; + \; \omega_g^2\, u_g(t) = \xi(t) \tag{49}$$

with ω_g and ζ_g denoting the filter (soil) natural frequency and damping ratio, and $\xi(t)$ a zero-mean, Gaussian white noise with one-sided spectral density $2\pi S_0$. The one-sided power spectral density of $z(t)$ is then

$$S_z(\omega) \; = \; S_0\, \frac{4\zeta_g^2\omega_g^2\omega^2 + \omega_g^4}{\left(\omega_g^2 - \omega^2\right)^2 + 4\zeta_g^2\omega_g^2\omega^2} \tag{50}$$

The governing rocking dynamics are defined in the state-space form

$$\dot{\mathbf{x}}(t) = \mathbf{Q}(t)\,\mathbf{x}(t) + \mathbf{q}(t) \tag{51}$$

with

$$\mathbf{Q}(t) = \begin{bmatrix} 0 & 1 & 0 & 0 \\ -\dfrac{k_{\mathrm{eq}}(t)}{m_{\mathrm{sdof}}} & -\dfrac{c_{\mathrm{eq}}(t)}{m_{\mathrm{sdof}}} & -\dfrac{q(t)\, mh\, \omega_g^2}{m_{\mathrm{sdof}}} & -\dfrac{2\, q(t)\, mh\, \zeta_g\omega_g}{m_{\mathrm{sdof}}} \\ 0 & 0 & 0 & 1 \\ 0 & 0 & -\omega_g^2 & -2\zeta_g\omega_g \end{bmatrix} \tag{52}$$

and

$$\mathbf{q}(t) = \begin{bmatrix} 0 & 0 & 0 & \xi(t) \end{bmatrix}^{\mathsf{T}}, \qquad \mathbf{x}(t) = \begin{bmatrix} \theta(t) & \dot{\theta}(t) & u_g(t) & \dot{u}_g(t) \end{bmatrix}^{\mathsf{T}} \tag{53}$$

Let the time-varying covariance of $\mathbf{x}(t)$ be

$$\mathbf{C}(t) = \mathbb{E}\left[\mathbf{x}(t)\,\mathbf{x}^{\mathsf{T}}(t)\right] = \begin{bmatrix} \sigma_\theta^2 & \sigma_{\theta\dot{\theta}} & \sigma_{\theta u_g} & \sigma_{\theta\dot{u}_g} \\ \sigma_{\theta\dot{\theta}} & \sigma_{\dot{\theta}}^2 & \sigma_{\dot{\theta}u_g} & \sigma_{\dot{\theta}\dot{u}_g} \\ \sigma_{\theta u_g} & \sigma_{\dot{\theta}u_g} & \sigma_{u_g}^2 & \sigma_{u_g\dot{u}_g} \\ \sigma_{\theta\dot{u}_g} & \sigma_{\dot{\theta}\dot{u}_g} & \sigma_{u_g\dot{u}_g} & \sigma_{\dot{u}_g}^2 \end{bmatrix} \tag{54}$$

Its evolution satisfies the time-evolving Lyapunov equation, Eq. (51) with

$$\mathbb{E}\left[\mathbf{q}(t)\,\mathbf{q}^{\mathsf{T}}(t)\right] = \begin{bmatrix} \mathbf{0}_{3\times3} & \mathbf{0}_{3\times1} \\ \mathbf{0}_{1\times3} & 2\pi S_0 \end{bmatrix} \tag{55}$$

Numerical time integration of this matrix differential equation yields the response second-order moments, including $\sigma_\theta^2(t)$ and $\sigma_{\dot{\theta}}^2(t)$.

2.7. Discussion on the proposed stochastic rocking dynamics technique

The technique combines a physics-based contact law with a blend of stochastic linearization, quasi-static condensation and Lyapunov formulation to deliver time-varying second-order response statistics for rocking dynamics. The contact force is cast on a continuously distributed spring-damper bed via an enhanced Hunt-Crossley-type law, in which classical velocity-dependent dissipation is complemented by coexisting linear and nonlinear stiffness components governed by a tunable parameter ε. This addition endows the restoring backbone with explicit amplitude dependence, enabling the model to represent both softening (e.g., geometric effects, toe degradation, interface yielding) and hardening effects (e.g., Hertz-type confinement) documented in the relevant literature (e.g., [34–36]). In practice, the formulation captures uplift asymmetry and the amplitude-frequency shift observed in rocking-effects that cannot be reproduced by calibrating nonlinear damping alone under a linear-stiffness assumption. For engineering application, the model parameters (including ε) are intended to be identified via calibration against measured force-indentation or moment-rotation backbones and energy dissipation trends, for instance from controlled rocking tests or well-instrumented response records.

The proposed formulation is intentionally parsimonious and nests prevalent models as limiting cases, thereby preserving backward compatibility and providing a transparent pathway for model selection. At the same time, the introduction of a single tunable nonlinear-stiffness parameter enhances the representational capacity of the contact/SSI backbone while maintaining the simplicity required for system identification and code-oriented applications [8,26,37]. Building on this contact description, the tailored stochastic linearization scheme yields closed-form, time-varying equivalent coefficients $c_{\text{eq}}(t)$ and $k_{\text{eq}}(t)$, whose evolution provides physically interpretable insight into the dissipation and restoring action as the response switches between no-uplift and uplift regimes.

From a computational standpoint, covariance propagation through a compact Lyapunov moment system avoids repeated nonlinear time integration and offers orders-of-magnitude reductions in effort relative to nonlinear response-history Monte Carlo when ensemble statistics are sought, while maintaining close agreement for the range of excitation intensities and foundation parameters examined. Overall, the proposed framework aims to balance fidelity and efficiency: it retains analytical tractability, enriches contact physics to accommodate softening or hardening backbones, recovers established rocking models as special cases, and delivers time-evolving second-order response statistics (e.g., variances of rotation and rotational velocity) at minimal computational cost.

Lastly, the combined use of stochastic linearization and quasi-static condensation may reasonably compromise accuracy under strongly nonlinear behavior. In particular, under very intense excitation-characterized by frequent uplift, strong intermittency, or near-toppling excursions-dynamic coupling effects may become significant and the accuracy of a condensed model can deteriorate, in which case full coupled nonlinear simulations may be required. Moreover, in the presence of very strong nonlinearities, it is well recognized in the broader random-vibration literature that stochastic linearization may also deteriorate and compromise accuracy (e.g., [8,27]). Further, retaining higher-order effects via perturbation-based expansions would render the piecewise-continuous damping and restoring moment across the no-uplift (inner) and uplift (outer) regimes algebraically cumbersome and largely unsuitable for further analytical treatment. Finally, the excitation model presumes Gaussianity of the base process; outside these assumptions, direct nonlinear simulation or alternative closure schemes may be preferable, albeit at the expense of computational efficiency.

3. Numerical analysis

This section evaluates the proposed semi-analytical stochastic dynamics framework on a set of representative nonlinear block rocking case studies. The excitation is modeled in two ways: (i) a time-modulated, unfiltered Gaussian white noise; and (ii) a time-modulated, filtered (Kanai-Tajimi-type) Gaussian white noise. In all cases, the block-foundation interaction follows the physics-based contact law of Section 2.1. Results are reported for several excitation intensities and four stiffness-nonlinearity configurations (hardening and softening), and are compared against Monte Carlo simulation (MCS) for validation. For the modulated unfiltered white noise case, the horizontal base acceleration is represented as a zero-mean Gaussian process with separable time-modulated power spectral density

$$S_{\ddot{x}}(\omega,t) \;=\; 2\pi\, S_0\, q^2(t) \tag{56}$$

where $S_0 > 0$ is the one-sided intensity parameter and $q(t)$ is a deterministic envelope. The envelope adopted here is

$$q(t) \;=\; 4\left(e^{-t/T_1} - e^{-t/T_2}\right), \qquad 0 < T_2 < T_1 \tag{57}$$

which produces a pulse-like build-up and decay typical of synthetic seismic inputs. The selected parameters are $T_1 = 4\,\text{s}$ and $T_2 = 2\,\text{s}$. In the proposed methodology formulation, the corresponding diffusion input in the Lyapunov moment equation (45) is given by (46). On the other hand, for the modulated filtered excitation case, the excitation reads $\ddot{x}(t) = q(t)\, z(t)$ where $z(t)$ is the output of a second-order linear filter driven by white noise (Section 2.6, Eqs. (47)–(55)) with $\zeta_g = 0.4$ and $\omega_g = 10.0$ rad/s. The approach allows exploration of frequency-content effects via the filter parameters while retaining a compact stochastic linearization Lyapunov format.

The selected prismatic block geometry follows refs. [19,23]. While these studies model the base-foundation interaction with nonlinearity confined to the damping term, the present study augments the restoring part via the physics-based contact law of Section 2.1. Four stiffness-nonlinearity configurations are examined for the same block geometry: Block Configuration 1 with $h = 0.21$ m, $b = 0.035$ m, $m = 8.67$ kg, and $\varepsilon = 6\times10^7$ m^{-2}; Block Configuration 2 with $h = 0.21$ m, $b = 0.035$ m, $m = 8.67$ kg, and $\varepsilon = -6\times10^5$ m^{-2}; Block Configuration 3 with $h = 0.21$ m, $b = 0.035$ m, $m = 8.67$ kg, and $\varepsilon = 2\times10^7$ m^{-2}; and Block Configuration 4 with $h = 0.21$ m, $b = 0.035$ m, $m = 8.67$ kg, and $\varepsilon = -2\times10^5$ m^{-2}. All configurations share the same geometric and inertial properties (m, b, h, I_{cm}) and gravity g. The uplift threshold $\theta_{\text{ul}} = mg/(2b^2k)$ is evaluated from the baseline stiffness. All other foundation parameters are identical across configurations; specifically, the contact coefficients are $k = 2.89\times10^7$ and $\lambda = 8.95\times10^8$ (refs. [19,23]). Each of configurations 1 and 2 is subjected to two intensity levels under the unfiltered modeling (S_0 varied in (56)–(57); Eqs. (39)–(46)), yielding four study cases. Analogously, each of configurations 3 and 4 is subjected to two intensity levels under the filtered modeling (Eqs. (47)–(55)), for a total of eight cases spanning regimes from predominantly no-uplift to appreciable uplift.

Accuracy is assessed by MCS. Ensembles of modulated unfiltered and filtered white-noise accelerations are synthesized via the spectral representation method [38]. For each realization, the coupled nonlinear rocking Eqs. (7)–(12) are solved by a Runge-Kutta scheme, and sample statistics are formed for direct comparison [39] with proposed stochastic linearization-based method predictions. In addition, the time-variant $c_{\text{eq}}(t)$ and $k_{\text{eq}}(t)$ are plotted to elucidate how dissipation and restoring trends evolve as the ensemble toggles between no-uplift and uplift contact states.

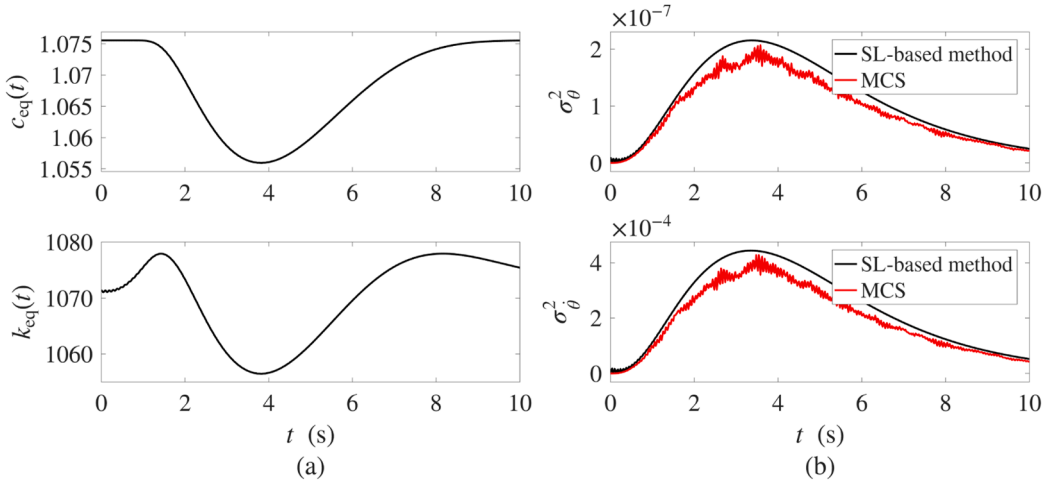

Fig. 2. Time histories of the equivalent linearized coefficients and response variances for modulated unfiltered white-noise excitation with hardening inner backbone; $S_0 = 2.4 \times 10^{-5}$ and $\varepsilon = 6 \times 10^7\ \mathrm{m}^{-2}$ (stochastic linearization-based method vs. Monte Carlo simulation with 1000 samples). (a) Equivalent damping $c_{eq}(t)$ (top) and equivalent stiffness $k_{eq}(t)$ (bottom). (b) Rotation variance $\sigma_\theta^2(t)$ (top) and rotational-velocity variance $\sigma_{\dot\theta}^2(t)$ (bottom).

3.1. Block configurations subjected to modulated unfiltered white-noise

Block Configuration 1. Fig. 2(a) shows the time histories of the equivalent damping and stiffness elements, $c_{eq}(t)$ and $k_{eq}(t)$, computed from the proposed stochastic linearization procedure for an excitation level $S_0 = 2.4 \times 10^{-5}$ with $\varepsilon = 6 \times 10^7\ \mathrm{m}^{-2}$. As the modulation $q(t)$ ramps up, the coefficients remain close to their inner-regime values (no uplift). Around the peak of the envelope, intermittent uplift becomes appreciable; the outer-regime contributions (the incomplete-gamma "tail" terms in Eq. (36)) reduce the equivalent stiffness, producing an effective softening. As the excitation decays, the system gradually returns toward the inner hardening level. The equivalent damping $c_{eq}(t)$ exhibits a mid-record dip, consistent with reduced contact length and diminished velocity-dependent dissipation during uplift phases. These trends match the physical picture: $\varepsilon > 0$ enhances the inner (no-uplift) backbone, whereas outer episodes always act to soften the ensemble response through loss of contact and redistribution of compressive resultants.

The corresponding time-varying response variances are plotted in Fig. 2(b). The stochastic linearization-based method predictions are benchmarked against MCS based on 1,000 modulated white-noise samples synthesized by the spectral representation method [38] and time integration of the nonlinear rocking equations. The proposed method tracks the rise-peak-decay evolution well for both $\sigma_\theta^2(t)$ and $\sigma_{\dot\theta}^2(t)$.

Fig. 3(a) reports $c_{eq}(t)$ and $k_{eq}(t)$ for the level $S_0 = 2.4 \times 10^{-3}$ (same ε). Relative to the milder case, the coefficients depart more markedly from their inner-regime baselines. In particular, $k_{eq}(t)$ exhibits a pronounced and sustained reduction during the mid-record window where uplift occupancy is largest; physically, frequent loss of contact and migration/shortening of the compression zone dominate the ensemble, overwhelming the inner hardening bias introduced by $\varepsilon > 0$. The damping $c_{eq}(t)$ shows a deeper trough for the same reason during uplift, the effective contact line contracts and the velocity-dependent dissipation decreases.

The associated second-order response statistics in Fig. 3(b) confirm the same narrative: both variances peak later and higher due to stronger excitation and increased outer-regime participation. Agreement between the stochastic linearization-based method and MCS shows a modest reduction in accuracy, yet remains satisfactory over the entire record. Across both intensities, the qualitative features of $k_{eq}(t)$ and $c_{eq}(t)$ are physically consistent: (i) a low-amplitude hardening bias at early times from the conservative stiffness nonlinear term acting in the inner regime; (ii) a mid-record softening of $k_{eq}(t)$ and a dip of $c_{eq}(t)$ driven by uplift, i.e., loss of contact and shorter compression zones; and (iii) relaxation back toward inner-regime values as the modulation fades. Minor oscillations visible at very early times are benign and stem from the envelope onset and the tail-integral (incomplete-gamma) contributions at extremely small variances; they vanish as the process develops. Overall, the trajectories of the equivalent elements encode a clear picture of how the ensemble toggles between no-uplift and uplift states, while the MCS comparisons substantiate that these elements provide a reliable, low-cost surrogate for the evolving second-order response statistics.

Block Configuration 2. Fig. 4(a) presents the equivalent coefficients $c_{eq}(t)$ and $k_{eq}(t)$ for a case with a softening inner backbone, $\varepsilon = -6 \times 10^5\ \mathrm{m}^{-2}$, under the moderate intensity $S_0 = 5 \times 10^{-4}$. Relative to Configuration 1, the early-time (inner-regime) level of $k_{eq}(t)$ is anticipated to exhibit a decreasing trend due to the reduction in restoring action induced by the conservative stiffness nonlinearity. As the envelope $q(t)$ grows and uplift intermittency increases, outer-regime contributions further depress $k_{eq}(t)$, producing a pronounced mid-record trough; the coefficient then recovers as the excitation decays. The damping $c_{eq}(t)$ exhibits the expected dip around the time window of largest uplift occupancy, reflecting a shortened contact line and reduced velocity-dependent dissipation. The accompanying

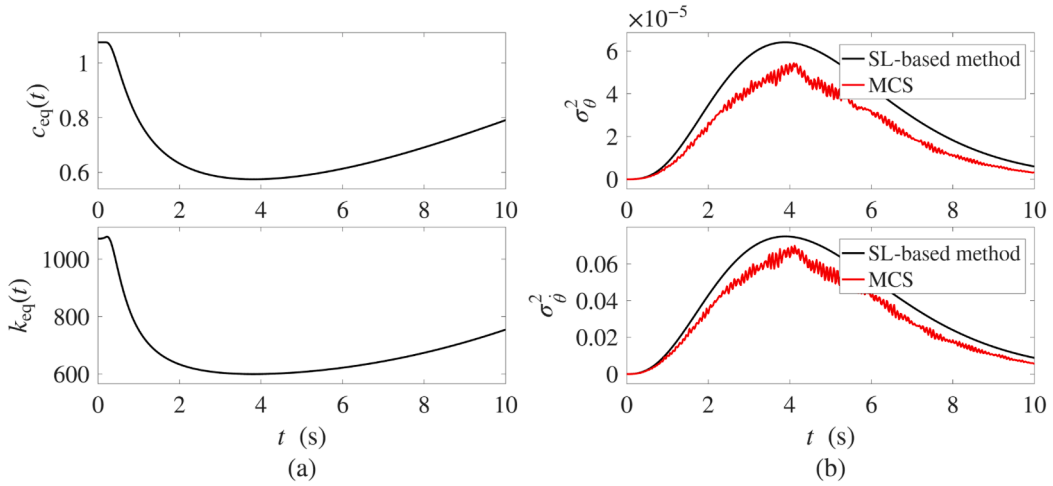

Fig. 3. Time histories of the equivalent linearized coefficients and response variances for modulated unfiltered white-noise excitation with hardening inner backbone; $S_0 = 2.4 \times 10^{-3}$ and $\varepsilon = 6 \times 10^7\ \mathrm{m}^{-2}$ (stochastic linearization-based method vs. Monte Carlo simulation with 1000 samples). (a) Equivalent damping $c_{eq}(t)$ (top) and equivalent stiffness $k_{eq}(t)$ (bottom). (b) Rotation variance $\sigma^2_\theta(t)$ (top) and rotational-velocity variance $\sigma^2_{\dot\theta}(t)$ (bottom).

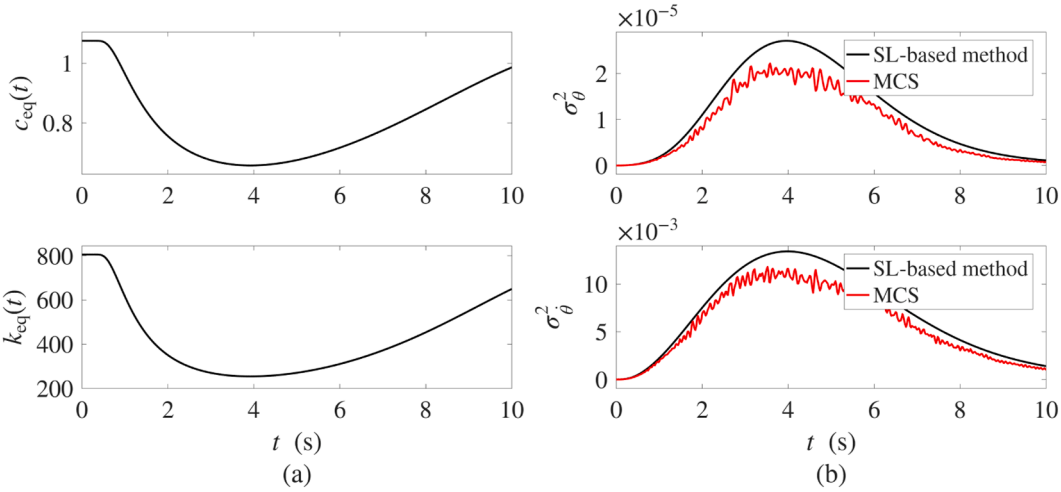

Fig. 4. Time histories of the equivalent linearized coefficients and response variances for modulated unfiltered white-noise excitation with softening inner backbone; $S_0 = 5 \times 10^{-4}$ and $\varepsilon = -6 \times 10^5\ \mathrm{m}^{-2}$ (stochastic linearization-based method vs. Monte Carlo simulation with 1000 samples). (a) Equivalent damping $c_{eq}(t)$ (top) and equivalent stiffness $k_{eq}(t)$ (bottom). (b) Rotation variance $\sigma^2_\theta(t)$ (top) and rotational-velocity variance $\sigma^2_{\dot\theta}(t)$ (bottom).

variances in Fig. 4(b) show acceptable agreement between the stochastic linearization-based solution and MCS: the proposed method curves capture the rise-peak-decay evolution, with a mild overprediction near peak intensity where the process is most nonlinear.

Fig. 5 reports the corresponding results for a stronger intensity $S_0 = 6.5 \times 10^{-4}$ (same ε). The increase in input level amplifies the contribution of uplift states, leading to a deeper and more sustained reduction of $k_{eq}(t)$ and a more pronounced trough in $c_{eq}(t)$. Consistently, both $\sigma^2_\theta(t)$ and $\sigma^2_{\dot\theta}(t)$ attain larger peaks and a slightly later timing. The proposed method predictions continue to track the MCS envelopes satisfactorily across the record, with differences concentrated near peak response, an expected outcome of the Gaussian closure when nonlinearity is stronger.

Across both intensities of Configuration 2, the qualitative behavior of the equivalent elements is consistent with a softening backbone in the inner regime ($\varepsilon < 0$) compounded by uplift in the outer regime: $k_{eq}(t)$ shows a sustained reduction and $c_{eq}(t)$ exhibits a concurrent dip. The satisfactory agreement with MCS indicates that the proposed semi-analytical framework provides reliable, low-cost estimates of the evolving second-order statistics even when softening tendencies dominate.

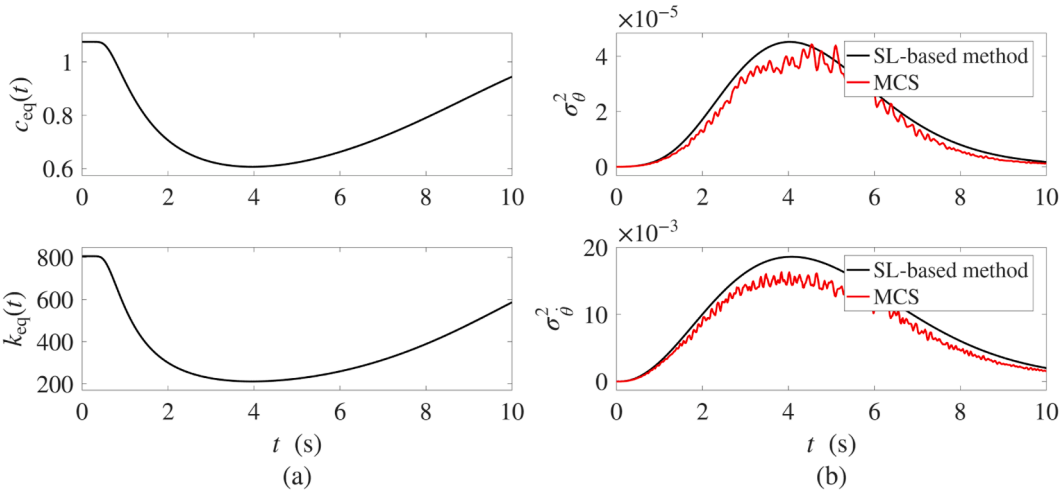

Fig. 5. Time histories of the equivalent linearized coefficients and response variances for modulated unfiltered white-noise excitation with softening inner backbone; $S_0 = 6.5 \times 10^{-4}$ and $\varepsilon = -6 \times 10^5$ m^{-2} (stochastic linearization-based method vs. Monte Carlo simulation with 1000 samples). (a) Equivalent damping $c_{eq}(t)$ (top) and equivalent stiffness $k_{eq}(t)$ (bottom). (b) Rotation variance $\sigma_\theta^2(t)$ (top) and rotational-velocity variance $\sigma_{\dot\theta}^2(t)$ (bottom).

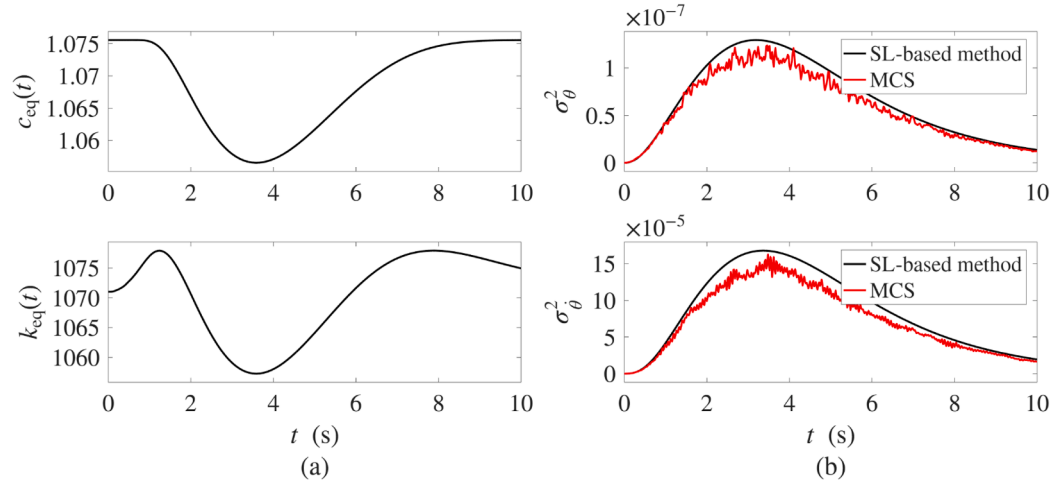

Fig. 6. Time histories of the equivalent linearized coefficients and response variances for modulated filtered white-noise excitation with hardening inner backbone; $S_0 = 2.5 \times 10^{-4}$ and $\varepsilon = 6 \times 10^7$ m^{-2} (stochastic linearization-based method vs. Monte Carlo simulation with 1000 samples). (a) Equivalent damping $c_{eq}(t)$ (top) and equivalent stiffness $k_{eq}(t)$ (bottom). (b) Rotation variance $\sigma_\theta^2(t)$ (top) and rotational-velocity variance $\sigma_{\dot\theta}^2(t)$ (bottom).

3.2. Block configurations subjected to modulated filtered white-noise

Block Configuration 3. Fig. 6 reports the time histories of the equivalent coefficients $c_{eq}(t)$ and $k_{eq}(t)$, together with the response variances $\sigma_\theta^2(t)$ and $\sigma_{\dot\theta}^2(t)$, for the filtered noise case with a hardening inner backbone, $\varepsilon = 6 \times 10^7$ m^{-2} and intensity $S_0 = 2.5 \times 10^{-4}$. At this moderate level and around the midpoint of the record, intermittent uplift becomes noticeable and produces a mild softening of the equivalent damping $c_{eq}(t)$, consistent with the reduction of instantaneous contact length under uplift. The stochastic linearization predictions of $\sigma_\theta^2(t)$ and $\sigma_{\dot\theta}^2(t)$ track the Monte Carlo results well across the rise-peak-decay phases, with the usual small deviations near the peak where nonlinearity is strongest. Compared with the non-filtered, modulated white-noise inputs (hardening backbone, $\varepsilon > 0$), the filtered cases here exhibit the same qualitative trend for the equivalent stiffness $k_{eq}(t)$: an early-time hardening bias (inner, no-uplift regime), a mid-record softening dip when uplift occupancy peaks, and a late-time recovery toward the inner baseline as the envelope decays. The main differences are quantitative: filtering concentrates energy near the soil/filter frequency, which shifts the timing and depth of the softening window, but the hardening-softening-hardening sequence persists.

Fig. 7 presents the same diagnostics for the higher intensity $S_0 = 4 \times 10^{-4}$ (same ε). The filtered input concentrates energy near the soil/filter frequency, increasing the occupancy of the uplift regime close to the envelope peak. Consequently, $k_{eq}(t)$ exhibits a

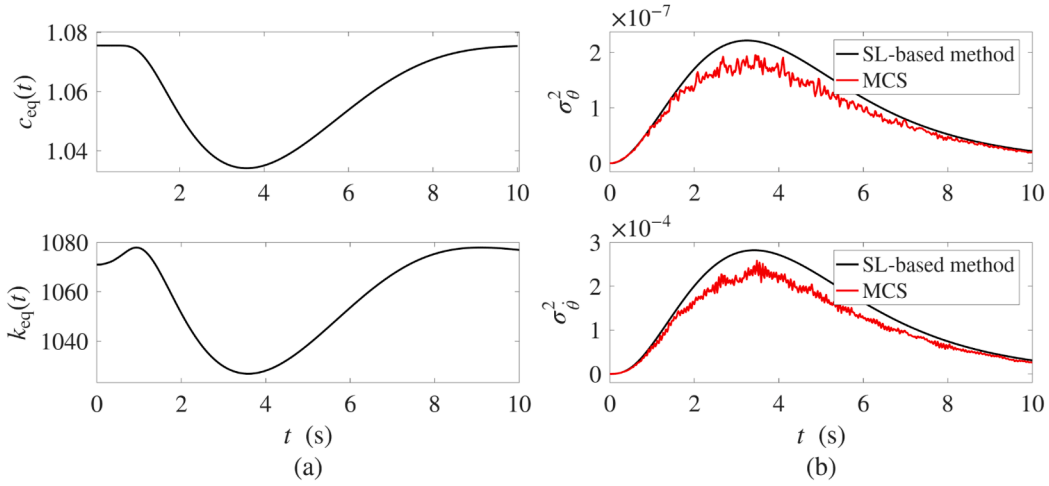

Fig. 7. Time histories of the equivalent linearized coefficients and response variances for modulated filtered white-noise excitation with hardening inner backbone; $S_0 = 4 \times 10^{-4}$ and $\varepsilon = 6 \times 10^7$ m^{-2} (stochastic linearization-based method vs. Monte Carlo simulation with 1000 samples). (a) Equivalent damping $c_{eq}(t)$ (top) and equivalent stiffness $k_{eq}(t)$ (bottom). (b) Rotation variance $\sigma_\theta^2(t)$ (top) and rotational-velocity variance $\sigma_{\dot\theta}^2(t)$ (bottom).

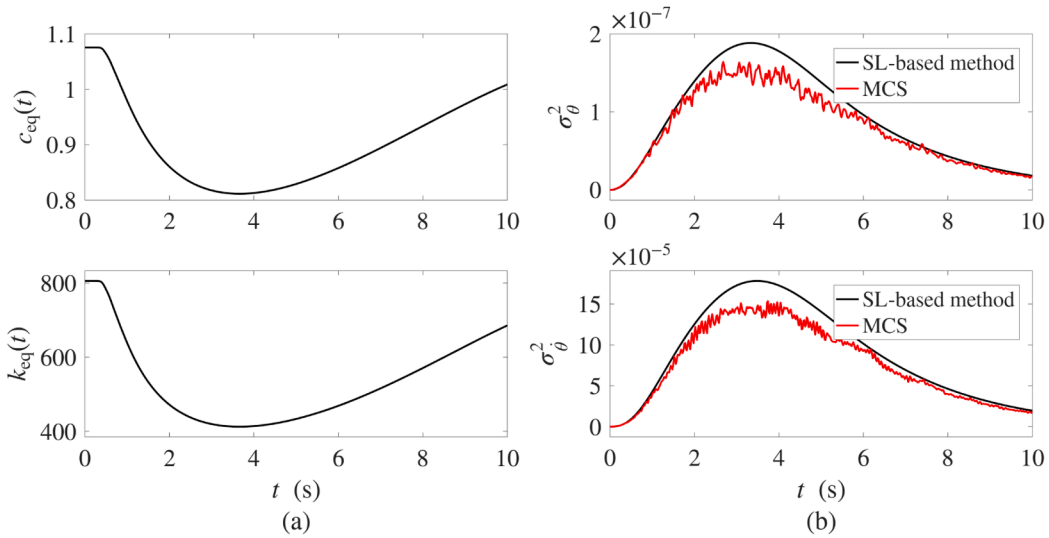

Fig. 8. Time histories of the equivalent linearized coefficients and response variances for modulated filtered white-noise excitation with softening inner backbone; $S_0 = 1.8 \times 10^{-4}$ and $\varepsilon = -6 \times 10^5$ m^{-2} (stochastic linearization-based method vs. Monte Carlo simulation with 1000 samples). (a) Equivalent damping $c_{eq}(t)$ (top) and equivalent stiffness $k_{eq}(t)$ (bottom). (b) Rotation variance $\sigma_\theta^2(t)$ (top) and rotational-velocity variance $\sigma_{\dot\theta}^2(t)$ (bottom).

deeper mid-record reduction and $c_{eq}(t)$ shows a more pronounced dip, both relaxing toward inner-regime values as the modulation fades. The second-order statistics rise to larger peaks, reflecting the stronger effective excitation; agreement between the proposed method and MCS remains satisfactory throughout.

Overall, for $\varepsilon > 0$ the inner (no-uplift) dynamics retain a hardening bias, while the filtered excitation promotes uplift-induced softening during the mid-record window. The equivalent elements capture this alternation cleanly, and the resulting evolving variances compare favorably with Monte Carlo benchmarks.

Block Configuration 4. Fig. 8 presents the equivalent coefficients $c_{eq}(t)$ and $k_{eq}(t)$ for a case with a softening inner backbone, $\varepsilon = -6 \times 10^5$ m^{-2}, under the moderate intensity $S_0 = 1.8 \times 10^{-4}$. The equivalent elements stay close to their inner-regime baselines except during the mid-record window, where uplift intermittency produces the familiar dip in both $c_{eq}(t)$ and $k_{eq}(t)$. The response variances $\sigma_\theta^2(t)$, $\sigma_{\dot\theta}^2(t)$ obtained from the proposed method follow the Monte Carlo estimates well: the rise-peak-decay timing matches, and peak levels are reproduced with minor, systematic overestimation near the maximum.

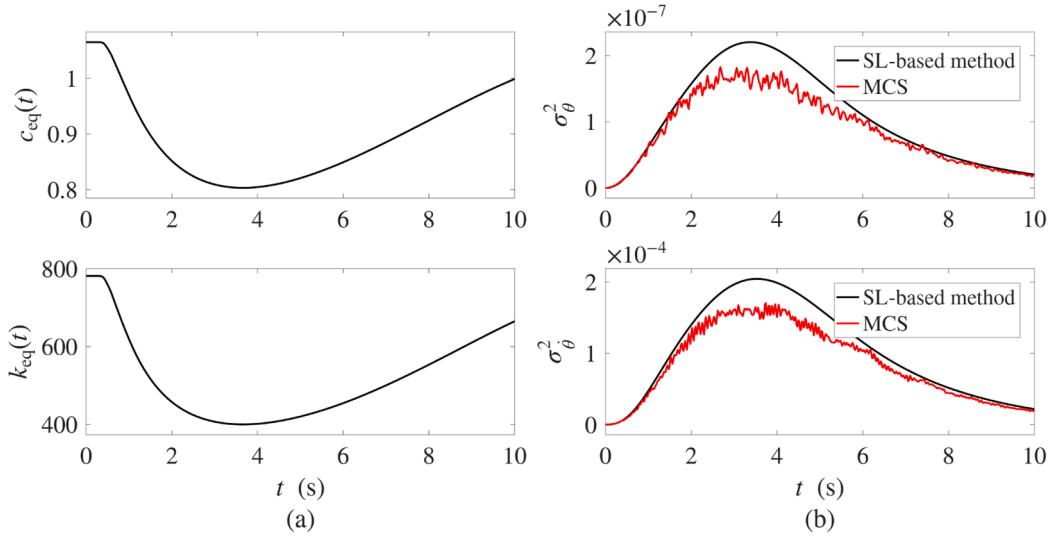

Fig. 9. Time histories of the equivalent linearized coefficients and response variances for modulated filtered white-noise excitation with softening inner backbone; $S_0 = 2.0 \times 10^{-4}$ and $\varepsilon = -6 \times 10^5\ \mathrm{m}^{-2}$ (stochastic linearization-based method vs. Monte Carlo simulation with 1000 samples). (a) Equivalent damping $c_{eq}(t)$ (top) and equivalent stiffness $k_{eq}(t)$ (bottom). (b) Rotation variance $\sigma_\theta^2(t)$ (top) and rotational-velocity variance $\sigma_{\dot\theta}^2(t)$ (bottom).

Increasing the intensity to $S_0 = 2.0 \times 10^{-4}$ (Fig. 9) amplifies the same trends without changing their character. The equivalent stiffness exhibits a deeper softening trough during the strongest portion of the record and then recovers towards its no-uplift level as the modulation decays, while $c_{eq}(t)$ shows a concurrent mid-record reduction consistent with a shortened contact line in the uplift regime. The predicted second-order statistics remain in satisfactory agreement with MCS across the entire time span.

For a softening backbone ($\varepsilon < 0$) under time-modulated unfiltered white noise, the equivalent stiffness $k_{eq}(t)$ typically shows an early effective softening as the envelope builds, followed by a recovery (apparent hardening) toward its inner-regime baseline as the excitation decays. The filtered cases reported here exhibit the same qualitative trajectory, initial softening, a mid-record trough during uplift, and late-time recovery while the filter mainly shifts the timing and slightly smooths the minimum due to its finite bandwidth. Thus, the trend of $k_{eq}(t)$ is consistent across filtered and non-filtered inputs when the backbone is softening; differences are chiefly in phase and depth rather than in character.

The time histories of $c_{eq}(t)$ and $k_{eq}(t)$, highlighting the influence of ε (softening/hardening) and the transition between inner (no-uplift) and outer (uplift) regimes. For excitations selected around a moderate-motion plateau, the proposed methodology yields second-order statistics in good agreement with the Monte Carlo simulations, while requiring orders-of-magnitude less computational effort. Differences increase as the response becomes strongly intermittent and non-Gaussian (e.g., near-toppling excursions). As the excitation level increases leads to nonlinear effects spreaded over a broader time window, reflecting stronger contact nonlinearity due to more pronounced uplift episodes and amplitude-dependent restoring effects.

3.3. Discussion of the generated results

This section interprets the time-varying equivalent stiffness $k_{eq}(t)$ and damping $c_{eq}(t)$ elements extracted by the stochastic linearization Lyapunov formulation, with emphasis on their evolution across no-uplift (inner) and uplift (outer) regimes and on the role of the cubic stiffness nonlinearity term.

In the inner regime (full contact), the restoring action is dominated by the linear Winkler-type term together with the added conservative stiffness nonlinearity ($\varepsilon \neq 0$). Positive ε produces an amplitude-dependent hardening backbone, $k_{eq}(t)$ tends to increase as the rotation variance grows whereas negative ε yields softening (reduction in k_{eq} with amplitude). This inner-regime trend is most pronounced early on, when uplift occupancy is low and the effective contact length is maximal. When uplift becomes appreciable, geometry and the excitation intensity take over: the compressed toe shortens and the moment arm evolves, causing an intrinsic softening even for $\varepsilon > 0$. In the equivalent expressions this appears through the outer-regime tail terms (with upper incomplete gamma functions) that reduce the net stiffness as the process spends more time beyond the uplift threshold. As a result, typical records show a "growth-then-decay" pattern for $k_{eq}(t)$: an initial hardening bump (inner physics) followed by a decay (outer geometry) as the response explores larger rotations. The timing of these phases aligns with peaks of the modulation $q(t)$ and with increases in the uplift occupancy

$$P_{\text{uplift}}(t) = \operatorname{erfc}\left(\frac{\theta_{\text{ul}}}{\sqrt{2}\,\sigma_\theta(t)}\right) \tag{58}$$

The equivalent damping inherits its structure from velocity-dependent contact dissipation acting over the instantaneous contact length. In the inner regime, $c_{\mathrm{eq}}(t)$ scales with the probability of full contact (via erf) and typically grows as the response builds up. Once uplift is activated, the effective contact shrinks and the outer contributions (via gamma incomplete function) weaken with increasing σ_θ, so $c_{\mathrm{eq}}(t)$ often exhibits a dip during intervals of strong uplift. In the proposed modeling, high uplift occupancy coincides with reduced equivalent damping because less of the interface is available to dissipate energy.

Both $k_{\mathrm{eq}}(t)$ and $c_{\mathrm{eq}}(t)$ track the excitation envelope $q(t)$: as the input intensity rises, higher $\sigma_\theta(t)$ pushes the system into the outer regime, triggering the stiffness decay and the damping dip (e.g., [40]); as the envelope recedes, the process returns to inner behavior and the coefficients relax toward baseline values. This co-evolution of coefficients and response explains the observed phase-like structure in time (e.g., early hardening vs. late softening for k_{eq}, mid-duration dip in c_{eq}). The time variation of the equivalent stiffness reflects the evolving mixture of inner (no-uplift) and outer (uplift) contact states in the ensemble. For $\varepsilon > 0$, a hardening offset emerges at low intensity when full contact dominates; as uplift occupancy increases near peak excitation, the outer-tail contributions in $K(\theta)$ reduce the equivalent stiffness (effective softening); and as the input intensity decays, the response gradually returns toward the inner hardening level. This alternation is therefore a statistical signature of contact-state transitions across the ensemble.

The sign and magnitude of ε primarily tune the inner-regime backbone:

- $\varepsilon > 0$: enhanced restoring moment at moderate amplitudes (hardening), delaying uplift onset and elevating the early peak in $k_{\mathrm{eq}}(t)$.
- $\varepsilon < 0$: reduced restoring at moderate amplitudes (softening), advancing uplift and flattening or inverting the early $k_{\mathrm{eq}}(t)$ rise.

Regardless of ε, sufficiently large rotations introduce geometric softening in the outer regime. Hence, ε shapes when and how strongly the trajectory enters uplift, while geometry dictates the late-time decay. This separation lends the parameters physical interpretability and supports data-driven identification: ε controls amplitude-dependent backbone in full contact; uplift geometry controls large-amplitude decay.

Across the considered cases, the proposed stochastic linearization-based predictions for the second-order statistics (variance of rotation, rotational velocity) match MCS trends: the timing and relative amplitude of the hardening bump in k_{eq}, the uplift-induced decay, and the damping dip are reproduced with good fidelity at a low computational cost. Simple diagnostics corroborate the mechanism: peaks in $P_{\mathrm{uplift}}(t)$ align with dips in $c_{\mathrm{eq}}(t)$ and with the onset of $k_{\mathrm{eq}}(t)$ decay; increasing $|\varepsilon|$ strengthens the inner-regime deviation from the linear baseline, while leaving the qualitative outer-regime softening intact.

The time histories $k_{\mathrm{eq}}(t)$ and $c_{\mathrm{eq}}(t)$ offer a compact, physically interpretable lens on the evolving rocking dynamics: they quantify the instantaneous restoring and dissipative capacity as the contact state changes in time. Practically, this supports performance assessment, parametric screening, and control concepts that hinge on when uplift occurs and how the interface dissipates at different amplitudes. Accuracy may deteriorate under stronger nonlinearity or far-from-Gaussian excitation, for which direct nonlinear simulation can be warranted. Within the examined ranges, however, the proposed stochastic linearization Lyapunov formulation captures the salient physics, inner hardening/softening, outer geometric softening, and uplift-driven damping, while remaining computationally lean.

4. Concluding remarks

This paper presented an integrated semi-analytical stochastic framework for the nonlinear rocking dynamics of rigid blocks on flexible foundations under time-varying stochastic base excitation. The approach combines a generalized physics-based contact/SSI formulation with quasi-static condensation, stochastic linearization, and Lyapunov-based covariance propagation to efficiently deliver time-evolving second-order response statistics. Within this unified setting, the adopted contact law remains parsimonious while introducing an explicitly amplitude-dependent conservative backbone and deformation-/rate-dependent dissipation, thereby accommodating backbone hardening or softening, uplift-induced asymmetry, and state-dependent stiffness and dissipation effects that cannot be captured by purely linear idealizations.

The initially coupled, piecewise nonlinear rocking equations are condensed into a single governing relation through a quasi-static condensation procedure. In doing so, suitable analytical expressions are derived for the piecewise-continuous restoring and damping moments, resulting in a unified yet accurate description of the rocking response across the no-uplift (inner) and uplift (outer) regimes. On this basis, a tailored stochastic linearization strategy embedded within a Lyapunov moment framework yields time-varying equivalent stiffness and damping elements that adapt to the evolving contact state, while offering physically interpretable insight into the dynamic character of the system.

Computationally, the proposed approach provides substantial advantages relative to direct simulation, since second-order response statistics are obtained from a compact Lyapunov system driven by a time-evolving power spectral density, thereby avoiding repeated time integration of the highly nonlinear equations. The numerical studies demonstrate close agreement with Monte Carlo simulations for the variances of rotation and rotational velocity over a range of excitation intensities and foundation parameters, supporting the method's accuracy and practical reliability within the targeted regime. From an engineering standpoint, the framework offers a concise tool for efficient rocking analysis under time-varying excitation and complex soil-structure interaction, enabling efficient assessment, parametric screening, and resilience-oriented studies.

CRediT authorship contribution statement

Ioannis P. Mitseas: Writing – review & editing, Writing – original draft, Visualization, Software, Project administration, Methodology, Funding acquisition, Conceptualization.

Data availability

Data will be made available on request.

Declaration of competing interest

The author declare that he has no known competing financial interests or personal relationships that could have appeared to influence the work reported in this paper.

Acknowledgment

The author gratefully acknowledge the support by the Hellenic Foundation for Research and Innovation (grant no. 1261).

Supplementary material

Supplementary material associated with this article can be found, in the online version at 10.1016/j.jsv.2026.119733.

References

[1] D. Konstantinidis, N. Makris, Experimental and analytical studies on the response of freestanding laboratory equipment to earthquake shaking, Earthq. Eng. Struct. Dyn. 38 (2009) 827–848.
[2] A.N. Kounadis, Seismic instability of free-standing statues atop multispondyle columns: a heuristic very stable system of ancient technology, Soil Dyn. Earthq. Eng. 119 (2019) 253–264.
[3] N. Makris, M.F. Vassiliou, Sizing the slenderness of free-standing rocking columns to withstand earthquake shaking, Arch. Appl. Mech. 82 (2012) 1497–1511.
[4] L. Gioiella, E. Tubaldi, F. Gara, L. Dezi, A. Dall'Asta, Modal properties and seismic behaviour of buildings equipped with external dissipative pinned rocking braced frames, Eng. Struct. 172 (2018) 807–819.
[5] C.-S. Yim, A.K. Chopra, J. Penzien, Rocking response of rigid blocks to earthquakes, Earthq. Eng. Struct. Dyn. 8 (6) (1980) 565–587.
[6] P.D. Spanos, A.S. Koh, Analysis of block random rocking, Soil Dyn. Earthq. Eng. 5 (1986) 178–183.
[7] R.N. Iyengar, C.S. Manohar, Rocking response of rectangular rigid blocks under random noise base excitations, Int. J. Non Linear Mech. 26 (6) (1991) 885–892.
[8] I.P. Mitseas, M. Beer, Modal decomposition method for response spectrum based analysis of nonlinear and non-classically damped systems, Mech. Syst. Signal Process. 131 (2019) 469–485.
[9] G.W. Housner, The behavior of inverted pendulum structures during earthquakes, Bull. Seismol. Soc. Am. 53 (1963) 403–417.
[10] H. Lin, S. Yim, Nonlinear rocking motions. II: overturning under random excitations, J. Eng. Mech. 122 (8) (1996) 728–735.
[11] I.N. Psycharis, P.C. Jennings, Rocking of slender rigid bodies allowed to uplift, Earthq. Eng. Struct. Dyn. 11 (1983) 57–76.
[12] A.S. Koh, P.D. Spanos, J.M. Roesset, Harmonic rocking of rigid block on flexible foundation, J. Eng. Mech. 112 (11) (1986) 1165–1180.
[13] A. Palmeri, N. Makris, Response analysis of rigid structures rocking on viscoelastic foundation, Earthq. Eng. Struct. Dyn. 37 (2008) 1039–1063.
[14] M.N. Chatzis, A.W. Smyth, Robust modeling of the rocking problem, J. Eng. Mech. 138 (2012) 247–262.
[15] R. Ceravolo, M.L. Pecorelli, L. Zanotti Fragonara, Semi-active control of the rocking motion of monolithic art objects, J. Sound Vib. 374 (2016) 1–16.
[16] P.A. Bońkowski, Z. Zembaty, M.Y. Minch, Engineering analysis of strong ground rocking and its effect on tall structures, Soil Dyn. Earthq. Eng. 116 (2019) 358–370.
[17] M.A. ElGawady, Q. Ma, J.W. Butterworth, J. Ingham, Effects of interface material on the performance of free rocking blocks, Earthq. Eng. Struct. Dyn. 40 (4) (2011) 375–392.
[18] J. Choi, S. Rhim, J.H. Choi, A general purpose contact algorithm using a compliance contact force model for rigid and flexible bodies of complex geometry, Int. J. Non Linear Mech. 53 (2013) 13–23.
[19] P.D. Spanos, A. Di Matteo, A. Pirrotta, M. Di Paola, Rocking of rigid block on nonlinear flexible foundation, Int. J. Non Linear Mech. 94 (2017) 362–374.
[20] G. Gilardi, I. Sharf, Literature survey of contact dynamics modelling, Mech. Mach. Theory 37 (10) (2002) 1213–1239.
[21] A. Di Matteo, A. Pirrotta, E. Gebel, P.D. Spanos, Analysis of block random rocking on nonlinear flexible foundation, Probab. Eng. Mech. 59 (2020) 103017.
[22] P. Frost, P. Cacciola, Rocking of rigid non-symmetric blocks standing on a horizontally-moving compliant base, Eng. Struct. 312 (2024) 118245.
[23] I.P. Mitseas, Y. Zhang, V.C. Fragkoulis, Risk assessment of block random rocking on nonlinear foundation subject to evolutionary seismic ground motion, Mech. Syst. Signal Process. 240 (2025) 113397.
[24] W. Goldsmith, Impact: The Theory and Physical Behaviour of Colliding Solids, Dover Publications, Incorporated, 1998.
[25] P. Frost, P. Cacciola, Dynamic cross-interaction between two adjacent rocking blocks, Soil Dyn. Earthq. Eng. 178 (2024) 108483.
[26] I.P. Mitseas, I.A. Kougioumtzoglou, A. Giaralis, M. Beer, A novel stochastic linearization framework for seismic demand estimation of hysteretic MDOF systems subject to linear response spectra, Struct. Saf. 72 (2018) 84–98.
[27] J.B. Roberts, P.D. Spanos, Random Vibration and Statistical Linearization, Courier Corporation, 2003.
[28] I.P. Mitseas, P. Ni, V.C. Fragkoulis, M. Beer, Survival probability surfaces of hysteretic fractional order structures exposed to non-stationary code-compliant stochastic seismic excitation, Eng. Struct. 318 (2024) 118755.
[29] J. Li, J. Chen, Stochastic Dynamics of Structures, John Wiley & Sons, 2009.
[30] A. Papoulis, S.U. Pillai, Probability, Random Variables, and Stochastic Processes, (4th ed.), McGraw-Hill, 2002.
[31] J. Xu, J. Li, Stochastic dynamic response and reliability assessment of controlled structures with fractional derivative model of viscoelastic dampers, Mech. Syst. Signal Process. 72 (2016) 865–896.
[32] G. Alotta, M. Di Paola, A. Pirrotta, Fractional Tajimi-Kanai model for simulating earthquake ground motion, Bull. Earthq. Eng. 12 (2014) 2495–2506.
[33] X. Ge, C. Li, I. Azim, J. Gong, Y. Li, Structural dynamic responses of linear structures subjected to Kanai-Tajimi excitation, Structures 34 (2021) 3958–3967.
[34] K.L. Johnson, Contact Mechanics, Cambridge University Press, 1987.
[35] I. Anastasopoulos, R. Kourkoulis, F. Gelagoti, E. Papadopoulos, Rocking response of SDOF systems on shallow improved sand: an experimental study, Soil Dyn. Earthq. Eng. 40 (2012) 15–33.
[36] O. Adamidis, G. Gazetas, I. Anastasopoulos, C. Argyrou, Equivalent-linear stiffness and damping in rocking of circular and strip foundations, Bull. Earthq. Eng. 12 (2014) 1177–1200.
[37] I.A. Kougioumtzoglou, P. Ni, I.P. Mitseas, V.C. Fragkoulis, M. Beer, An approximate stochastic dynamics approach for design spectrum-based response analysis of nonlinear oscillators with fractional derivative elements, Int. J. Non Linear Mech. 146 (2022) 104178.
[38] M. Shinozuka, G. Deodatis, Simulation of stochastic processes by spectral representation, ASME. Appl. Mech. Rev. 44 (4) (1995) 191–204.
[39] P. Ni, I.P. Mitseas, V.C. Fragkoulis, M. Beer, Spectral incremental dynamic methodology for nonlinear structural systems endowed with fractional derivative elements subjected to fully non-stationary stochastic excitation, Struct. Saf. 111 (2024) 102525.
[40] I.A. Kougioumtzoglou, Y. Zhang, M. Beer, Softening Duffing oscillator reliability assessment subject to evolutionary stochastic excitation, ASCE-ASME J. Risk Uncertain. Eng. Syst. Part A: Civil Eng. 2 (2) (2015) 04015002.